NPL
National Physical Laboratory

NPL REPORT AS 82

An investigation of the matrix sensitivity of refinery gas analysis using gas chromatography with flame ionisation detection

Valerio Ferracci
Andrew S. Brown
Peter M. Harris
Richard J.C. Brown

DECEMBER 2013

National
Measurement
System

An investigation of the matrix sensitivity of refinery gas analysis using gas chromatography with flame ionisation detection

Valerio Ferracci, Andrew S. Brown, Peter M. Harris,
Richard J.C. Brown

ABSTRACT

The response of a flame ionisation detector (FID) to methane, ethane, propane, *i*-butane and *n*-butane in a series of multi-component synthetic gas mixtures was analysed to investigate a possible matrix sensitivity. The analysis of the results showed a significant impact of changes in atmospheric pressure and detector drift on the instrument response: a procedure to account for these effects was devised and its use is recommended for future work performed on the instrument. A dependence of the instrument response on the component amount fraction was observed but this was not inconsistent with the results from other FIDs. No significant effects of four selected physical properties of the gas (molar weight, molar volume, density, viscosity) on the instrument response were observed.

ISSN 1754-2928

National Physical Laboratory
Hampton Road, Teddington, Middlesex, TW11 0LW

Approved on behalf of NPLML by Dr Michael Adeogun, Head of Analytical Science Division.

CONTENTS

1 INTRODUCTION

Refinery gases are complex mixtures of hydrocarbons, hydrogen and non-combustible gases (*e.g.* CO, CO_2, N_2, He, *etc*.), obtained as a by-product of crude oil refining and typically used as an energy source in other processes. Critically, the composition of refinery gas depends on a series of factors, such as the oil it originates from and the processes it has undergone.

Carbon trading measures, as detailed in the EU emissions trading scheme,[1] are currently driving the need to establish the carbon content and calorific value of the intermediate products of refinery processes, including refinery gas. This can be achieved only when the composition of refinery gas is accurately characterised.

Gas chromatography is usually the analytical technique employed to identify the composition of emissions from the petroleum industry, including refinery gas. One method for refinery gas analysis by means of gas chromatography has been recently published as a European standard;[2] this method involves the separation of the components of the gaseous mixture and the subsequent quantification of the hydrocarbon content of the gas by means of flame ionisation detection (FID) and of other components (N_2, CO, CO_2, O_2, He, H_2) *via* thermal conductivity detection (TCD).

In addition, National Measurement Institutes have developed traceable reference gas mixtures and methods for refinery gas analysis; their capabilities have been compared in an international comparison exercise arranged by the CCQM GAWG,[3] in which all the analytical methods employed involved gas chromatography with FID and TCD.

In all cases, a careful characterisation of the instrument response is crucial to accurately identify the composition of unknown mixtures against standards. As specified in Annex B of BS EN 15984:2011,[2] the response of a chromatographic detector can be considered linear when it remains constant within a specified variation (typically ± 5%, but this can be smaller for high-accuracy applications) over a range of compound concentrations or mass flows; however a degree of non-linearity is known to affect the response of both flame ionisation and thermal conductivity detectors. A series of preliminary experiments indicated a possible matrix sensitivity of the flame ionisation detector (FID) used for refinery gas analysis, with the detector response to specific hydrocarbons varying by as much as 4%. The present work aimed to investigate the sensitivity of the FID to a series of different gas mixtures, thus allowing the study of the instrument response to changes in parameters such as gas composition, density and viscosity.

2 EXPERIMENTAL

The composition of a series of synthetic gas mixtures containing C_1-C_6 hydrocarbons was analysed using a refinery gas analyser gas chromatography (GC) system coupled with flame ionisation detection (FID). A description of the apparatus and experimental procedure used are given below.

2.1 REFINERY GAS ANALYSER

The refinery gas analyser (Analytical Control Hi-Speed RGA)[4] consisted of three separate sampling channels: one channel was coupled to a flame ionisation detector (FID) while the remaining two were equipped with thermal conductivity detectors (TCD). The present work focused only on the response of the FID channel, hence a description of this channel alone is given in this section.

The FID channel consisted of a sample loop, a six-port gas sampling valve (Valve 1), a six-port back flush valve (Valve 2), a capillary pre-column (Column 1: 3 m long capillary column with a non-polar stationary phase - 100 % dimethylpolysiloxane (SPB-1). Internal diameter = 0.32 mm, film thickness = 4 μm) and a capillary aluminumoxide PLOT column (Column 2: 25 m long alumina PLOT column.

Internal diameter = 0.32 mm, film thickness = 8 μm), configured in sequence, as illustrated in Figure 1. Helium gas (BIP, Air Products) was used as the carrier gas. To introduce the sample into the system, Valve 1 was switched so that the contents of the sample loop were injected into the carrier gas flow. The sample then flowed through Column 1, where a pre-separation of the components occurred, with the heavier hydrocarbons travelling down the column more slowly than lighter ones. Prior to the elution of *n*-hexane and heavier hydrocarbons from Column 1 onto Column 2, the backflush of Column 1 was activated by switching Valve 2: this caused the flow through Column 1 to be reversed and Column 2 to be placed behind Column 1 in the flow-sequence. This allowed heavier hydrocarbons, the long retention times of which would have otherwise led to lengthy experimental runs, to elute before lighter ones, thus reducing the duration of the run.

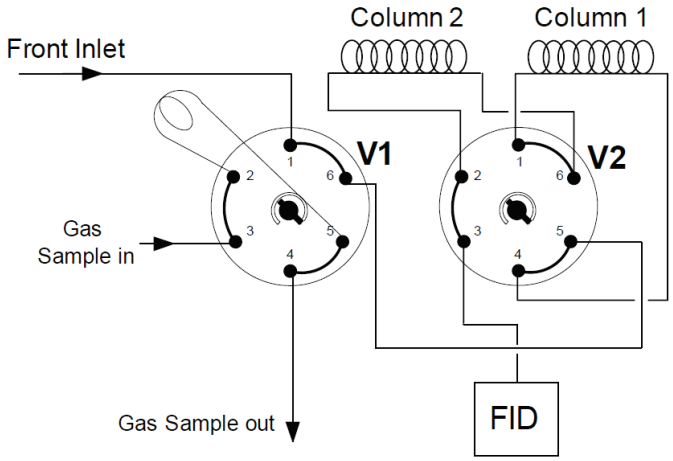

Figure 1 Schematic representation of the FID channel of the Refinery Gas Analyser (RGA) used in the current work. See text for details. Adapted from reference 4.

The FID was kept at a temperature of T = 280 °C with a hydrogen flow of 35 mL/min, an air flow of 350 mL/min and a make-up flow of nitrogen of 15 mL/min. Valve 1 was located in a dedicated valve oven which was kept at a temperature of T = 65 °C, whilst Columns 1 and 2 and Valve 2 were located in the main GC oven: in each run, the temperature of the GC oven was programmed so that the initial temperature of T = 30 °C was held for the first 1.4 min; the oven temperature was then increased to T = 80 °C at a rate of dT/dt = 30 °C/min, then held at T = 80 °C for 5 min. Sample flow was typically 25 ± 0.5 mL/min; the contents of the sample loop were injected into the FID channel by switching Valve 1 at t = 0.11 min after the start of the run. Valve 1 was then switched again at t = 0.6 min, by which time all the contents of the sample loop were transferred onto the FID channel. Backflush of Column 1 was activated by switching Valve 2 at t = 0.55 min.

2.2 GAS MIXTURE COMPOSITION AND PHYSICAL PROPERTIES

12 gas mixtures were identified as suitable for this study. These contained, among other components, methane, ethane, propane, *i*-butane and *n*-butane; crucially, the amount fraction of these components varied from one mixture to the other. These mixtures were prepared gravimetrically at NPL using 'pure' gases, 'pure' liquids and pre-mixtures, each component added separately using either small transfer vessels or direct gas transfer. A full purity analysis was carried out on each 'pure' gas or liquid. The gravimetric amount of each component and the uncertainty associated with it were calculated from the mass of each component added, its relative molar mass and purity analysis data using the NPL Software GravCalc2 [5] (in accordance with ISO 6142 [6]). The gravimetric composition of the mixtures used is given in Table 1; the relative uncertainties associated with the amount fractions in Table 1 are reported in Table 2.

Table 1 Gravimetric composition of the gas mixtures used. Amount fractions are given in units of % mol/mol. The QA is the quality assurance standard, as described in Section 2.3.

Component	QA	Sample 1	Sample 2	Sample 3	Sample 4	Sample 5	Sample 6	Sample 7	Sample 8	Sample 9	Sample 10	Sample 11
Methane	64.311	49.150	57.049	26.635	52.213	35.045	10.011	10.419	67.773	30.460	18.318	87.110
Ethane	0.8965	34.595	1.2367	24.775	4.8941	7.3868			10.297	27.986	17.627	0.5229
Ethene				6.9793	3.4529		4.1951	1.0797		11.982	5.2262	
Propane	0.0790	12.287	1.6699	3.9717	9.9248	4.9835	4.3354	2.8642	1.5491	0.0255	7.9808	7.9741
Propene				0.8915	4.8899			2.9916		6.9895		
***i*-butane**	0.0113		0.0634			0.8449	2.9481		0.3394		4.1179	1.2160
***n*-butane**	0.0057		0.0639			0.8708	2.9345	3.9903	0.4171		5.9055	1.7032
1-butene											0.3219	
***neo*-pentane**			0.0102									0.2002
***i*-pentane**	0.0017		0.4490			0.3499					0.7819	0.0794
***n*-pentane**	0.0007		0.4557			0.3681					0.8004	0.0145
***n*-hexane**			0.0435			0.1023						0.0602
***cis*-2-butene**											0.3175	
***trans*-2-butene**											0.3187	
Nitrogen	16.913	3.9651	25.213	4.0131	1.7676	23.215	52.567	34.598	10.002	11.814	5.1117	0.6409
Oxygen	0.5084										0.1307	
Hydrogen				27.058	15.263	10.589	9.7932	40.543	7.8615		32.487	
Helium			0.2321									0.0105
Argon							2.1485					
Carbon monoxide				3.0240	6.6121	8.0654	11.064	3.5123	1.2373	7.7504		
Carbon dioxide	17.272		13.511	2.6514	0.9820	8.1766			0.5238	2.9924	0.5477	0.4656

Table 2 Relative percentage uncertainties in the gravimetric composition of the gas mixtures listed in Table 1. These uncertainties are stated at a level of $k = 2$, providing a level of confidence of approximately 95 %. The QA is the quality assurance standard, as described in Section 2.3.

Component	QA	Sample 1	Sample 2	Sample 3	Sample 4	Sample 5	Sample 6	Sample 7	Sample 8	Sample 9	Sample 10	Sample 11
Methane	0.009	0.024	0.027	0.053	0.021	0.029	0.144	0.171	0.010	0.025	0.207	0.008
Ethane	0.172	0.027	0.117	0.050	0.094	0.072			0.036	0.021	0.191	0.036
Ethene				0.066	0.139		0.208	0.769		0.042	0.296	
Propane	0.044	0.042	0.300	0.071	0.042	0.074	0.130	0.215	0.109	4.001	0.206	0.082
Propene				0.250	0.072			0.215		0.051		
***i*-butane**	0.214		0.428			0.029	0.147		0.024		0.234	0.033
***n*-butane**	0.421		0.384			0.029	0.147	0.152	0.023		0.208	0.032
1-butene											0.212	
***neo*-pentane**			0.221									0.158
***i*-pentane**	0.136		0.685			0.100					0.274	0.154
***n*-pentane**	0.228		0.675			0.098					0.272	0.786
***n*-hexane**			5.906			0.050						0.066
***cis*-2-butene**											0.236	
***trans*-2-butene**											0.236	
Nitrogen	0.026	0.178	0.042	0.092	0.272	0.032	0.026	0.118	0.030	0.042	0.296	0.094
Oxygen	0.180										0.429	
Hydrogen				0.124	0.078	0.076	0.096	0.172	0.090		0.374	
Helium			0.192									0.214
Argon							0.289					
Carbon monoxide				0.116	0.074	0.070	0.078	0.256	0.214	0.064		
Carbon dioxide	0.018		0.048	0.090	0.314	0.048			0.018	0.106	0.184	0.072

Physical properties of each mixture were calculated using the Microsoft Excel add-in software GasVLe (GL Noble Denton). The software used the Redlich-Kwong-Soave (RKS) [7, 8] equation of state to calculate the physical properties of the mixtures from their gravimetric composition. In particular, the present study investigated the effects of different molar weight, density, molar volume and viscosity of the mixtures on the FID response as these were recognised as the fundamental properties of a gas mixture which might affect the response of the analyser. The values of these properties for each mixture are illustrated in Table 3.

Table 3 Physical properties of the 11 gas mixtures analysed in the present work. The uncertainties shown are at the $k = 2$ level, and their source is discussed in Section 3.4.

Sample No.	Molar Weight / g mol^{-1}	Density / mol m^{-3}	Molar Volume / 10^{-3} m^3 mol^{-1}	Viscosity / 10^{-2} mPa·s
1	24.817 ± 0.025	41.222 ± 0.041	24.258 ± 0.024	1.021 ± 0.051
2	24.051 ± 0.024	41.104 ± 0.041	24.328 ± 0.024	1.256 ± 0.063
3	19.491 ± 0.019	41.124 ± 0.041	24.316 ± 0.024	1.099 ± 0.055
4	20.338 ± 0.020	41.132 ± 0.041	24.312 ± 0.024	1.119 ± 0.056
5	24.219 ± 0.024	41.105 ± 0.041	24.327 ± 0.024	1.263 ± 0.063
6	26.995 ± 0.027	41.073 ± 0.041	24.346 ± 0.024	1.480 ± 0.074
7	18.309 ± 0.018	41.049 ± 0.041	24.360 ± 0.024	1.293 ± 0.065
8	18.629 ± 0.019	41.106 ± 0.041	24.327 ± 0.024	1.136 ± 0.057
9	26.413 ± 0.026	41.184 ± 0.041	24.281 ± 0.024	1.119 ± 0.056
10	23.100 ± 0.023	41.182 ± 0.041	24.281 ± 0.024	1.093 ± 0.055
11	19.994 ± 0.020	41.147 ± 0.041	24.303 ± 0.024	1.085 ± 0.054

2.3 EXPERIMENTAL PROCEDURE

One of the mixtures was chosen as the quality assurance (QA) standard, used to characterise the detector drift. This procedure is extensively described in the literature [9] and is briefly summarised in Section 3 below. From this point on, the QA is differentiated from the remaining 11 mixtures, referred to as "samples". The same QA was used throughout the series of experiments.

Repeat measurements of each sample mixture were performed in groups of three interspersed with one QA measurement as follows: QA-sample-sample-sample-QA-sample-sample-sample-QA-*etc*., for a total of 41 runs per sample mixture (30 of the actual sample, 11 of the QA), for an overall duration of approximately 8 hours. Therefore only one sample mixture was analysed each day.

3 DATA ANALYSIS

3.1 INTRODUCTION

The peak area of a component i, A_i, measured by gas chromatography is proportional to the amount fraction of that component in the mixture, x_i, according to the relationship:

$$A_i = RF_i \times x_i \qquad (1)$$

where RF_i indicates the response factor of the detector to component i. By rearranging equation (1), response factors can be calculated for all components in each mixture from the integrated peak areas (which are measured experimentally) and the amount fractions of each component (which are known from the calculations associated with the gravimetric preparation of each gaseous mixture). However, before response factors were calculated, two corrections were applied to the measured peak areas, one accounting for fluctuations in atmospheric pressure and the other accounting for detector drift.

3.2 PRESSURE CORRECTION

Changes in atmospheric pressure during the experiments affected the number of molecules injected into the analyser from a sample loop with a fixed volume. Therefore, all integrated areas were normalised to standard pressure (101 325 Pa) according to the relationship:

$$A_i' = A_i \Big/ \frac{p_{atm}}{p^\circ} \qquad (2)$$

where A_i' is the pressure-corrected area for component i, p° = 101 325 Pa and p_{atm} is the atmospheric pressure at the time of injection as reported by the NPL online barograph.[10]

3.3 DRIFT CORRECTION

As measurements of each sample mixture took place over a period of eight hours, a temporal drift in the detector's response was observed. The QA was used to quantify and correct for this drift by calculating a drift factor, defined as the fractional deviation of each integrated area for the components in the QA from the average of the integrated areas of the same component in the QA measured over a single day; therefore, for component i:

$$drift\ factor = A_i'(\mathrm{QA}) \,/\, \bar{A}_i'(\mathrm{QA}) \qquad (3)$$

where $A_i'(\mathrm{QA})$ is the pressure-corrected area for component i in the QA and $\bar{A}_i'(\mathrm{QA})$ is the average of the pressure-corrected areas for component i in the QA. Note that the areas used in the drift correction have already been corrected for changes in atmospheric pressure. As 11 measurements of the QA were carried out for each sample (*i.e.* each day), each component in the QA gave rise to 11 drift factors. A quadratic function typically provided a suitable representation of the temporal behaviour of drift factors: this function was least-squares fitted to data consisting of the drift factors for methane, ethane, propane, *iso*-butane and *n*-butane against time, and then used to correct the signal measured for the sample mixture on the same day, according to the relationship:

$$A_i''(\mathrm{sample}) = A_i'(\mathrm{sample}) \,/\, \varepsilon_{drift}(t) \qquad (4)$$

where $A_i''(\mathrm{sample})$ is the pressure- and drift-corrected area for component i in the sample mixture and $\varepsilon_{drift}(t)$ is the drift function calculated for the time of sample injection t. This correction assumed that the detector drift affected the QA and sample mixtures in an identical fashion. Figure 2 illustrates the drift correction carried out for the measured methane signal from Sample 5.

3.4 CALCULATION OF RESPONSE FACTORS

The average pressure- and drift-corrected areas for each component in the sample, $\bar{A}_i''(\mathrm{sample})$, were then divided by the component amount fraction to calculate the response factor for component i:

$$RF_i(\mathrm{sample}) = \bar{A}_i''(\mathrm{sample}) \,/\, x_i \qquad (5)$$

The response factors for the components in a particular sample mixture, $RF_i(\mathrm{sample})$, were

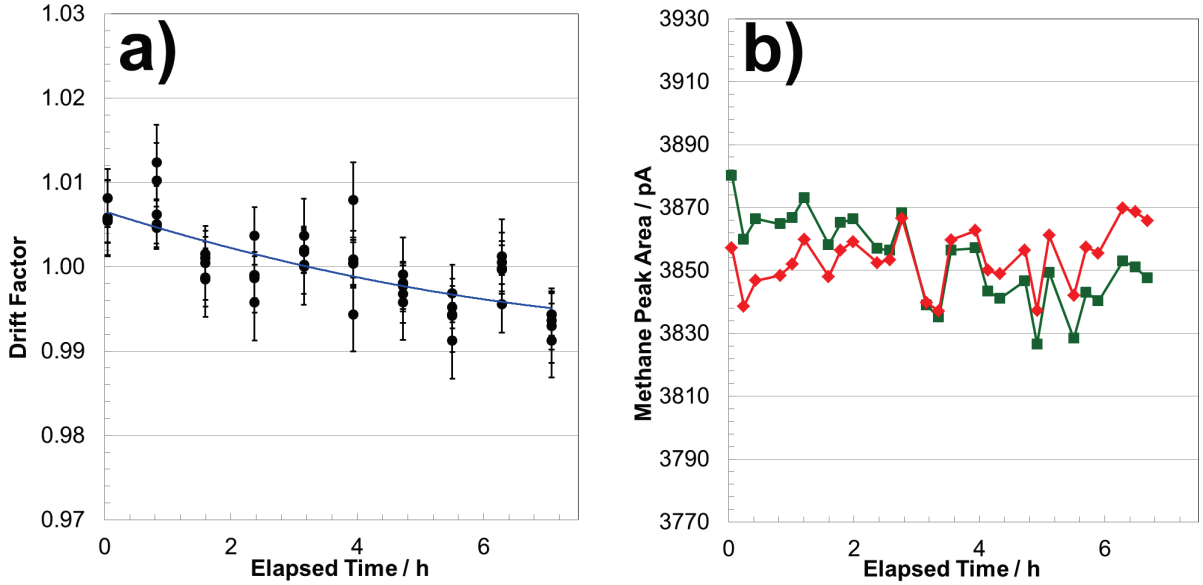

Figure 2 a) Typical plot of drift factors against elapsed time (black circles) with the least-squares fitted drift function (blue line); the magnitude of the error bars on the data points reflects the relative standard deviation associated with $\bar{A}_i'$(QA); b) effects of drift correction on the peak areas for methane from Sample 5, showing the pressure-corrected areas (in green) as well as the pressure- and drift-corrected areas (in red).

accompanied by the response factors for the components of the QA measured on the same day, RF_i(QA):

$$RF_i(\mathrm{QA}) = \bar{A}_i'(\mathrm{QA}) / x_i \qquad (6)$$

This allowed calculation of the *ratio* of the response factors for sample and QA component *i* measured on the same day, RRF_i:

$$RRF_i = \frac{RF_i(\mathrm{sample})}{RF_i(\mathrm{QA})} \qquad (7)$$

This procedure effectively accounted for any day-to-day change in the sensitivity of the detector.

In the chromatograms of sample mixtures where one or both of the butane species were present at amount fractions higher than 1 %, some degree of co-elution of the two components was observed. This was the case particularly for mixtures 6, 7, 10 and 11. The co-elution had an obvious effect on accurately determining the integrated peak areas, as it was not possible to accurately integrate the co-eluting peaks, in turn affecting the values of the response factor for the butane species and, ultimately, the ratio of response factors. One solution to this issue would have been to delay or slow down the temperature increase of the GC oven in each experimental run, leading to a better separation of the two peaks; however, the duration of each run would have increased, thus reducing the number of runs performed each day and therefore the amount of experimental data. Moreover, the chromatography of other components would have also been affected, for instance causing peak broadening. For the purposes of this study, *i*- and *n*-butane were treated as one component and, in the data analysis for the calculation of the ratio of response factors, the peak areas of the two components were added together, as well as their gravimetric amount fractions. This was justified by the fact that the response factors of *i*- and *n*-butane were nominally identical.

RRF values obtained for the 11 sample mixtures are given in Table 4, along with their associated uncertainties. Details of the evaluation of uncertainties are given in Section 3.5 below. *RRF* values from each sample mixture were subsequently used to ascertain whether the amount fraction of a component, or the physical properties of a sample mixture, had an effect on the instrument response.

Table 4 *RRF* values for the components in the 11 sample mixtures studied. The results for *i*-butane and *n*-butane are presented as one component for the reasons elucidated in Section 3.4. The uncertainties shown are at the $k = 2$ level and inflated by 12 %, as discussed in Section 3.5. However these uncertainties were additionally increased (typically by a factor of 2) following the chi-squared test, as also discussed in Section 3.5.

Sample No.	Methane	Ethane	Propane	*i*-butane + *n*-butane
1	1.0083 ± 0.0024	0.9874 ± 0.0031	0.9941 ± 0.0027	–
2	1.0025 ± 0.0032	0.9965 ± 0.0040	1.0021 ± 0.0049	1.0037 ± 0.0056
3	1.0044 ± 0.0027	0.9819 ± 0.0033	0.9883 ± 0.0043	–
4	1.0020 ± 0.0033	0.9955 ± 0.0041	0.9933 ± 0.0042	–
5	1.0064 ± 0.0030	0.9948 ± 0.0035	0.9954 ± 0.0047	1.0079 ± 0.0044
6	1.0157 ± 0.0024	–	0.9972 ± 0.0034	1.0015 ± 0.0033
7	1.0048 ± 0.0031	–	0.9889 ± 0.0032	1.0002 ± 0.0039
8	0.9971 ± 0.0025	0.9926 ± 0.0032	0.9973 ± 0.0041	–
9	1.0153 ± 0.0025	0.9930 ± 0.0031	–	–
10	1.0109 ± 0.0034	0.9886 ± 0.0037	0.9924 ± 0.0043	0.9918 ± 0.0042
11	0.9947 ± 0.0040	0.9940 ± 0.0043	0.9932 ± 0.0042	1.0056 ± 0.0041

3.5 SOURCES AND PROPAGATION OF UNCERTAINTY IN THE MEASURED AREAS

The standard uncertainties associated with the average pressure- and drift-corrected areas for component i in a sample mixture, $u(\bar{A}_i''(\text{sample}))$, and in the QA, $u(\bar{A}_i'(\text{QA}))$, were calculated as the standard errors of the mean values:[11]

$$u\left(\bar{A}_i''(\text{sample})\right), u\left(\bar{A}_i'(\text{QA})\right) = \frac{\sigma}{\sqrt{n}} \qquad (8)$$

where σ is the standard deviation of the areas measured for a particular component in a mixture and n is the number of measurements carried out for that mixture. Expanded uncertainties were determined by multiplying the standard uncertainties listed above by a coverage factor of two ($k = 2$), corresponding to a level of confidence of approximately 95 %.

A crucial assumption in the use of the standard error of the mean is that the repeated measured values for each component in a mixture are obtained independently, which is the case for A_i and A_i'. However drift correction introduces correlation associated with the A_i'' values as a result of the way drift factors (and the subsequent drift function) are calculated (equations 3 and 4). An analysis (described below) indicated that correlation gave rise to an inflation in the uncertainty associated with the final *RRF* values of about 12 %. The data analysis undertaken to obtain values for the *RRF* (equation 7) from the pressure-corrected area for component i in a sample mixture can be described by the following (computational) steps:

1. A transformation from (i) the pressure-corrected values $A_i'(\text{QA})$, $i = 1, \ldots, 5$, for all five components of the QA, and (ii) the pressure-corrected values $A_i'(\text{sample})$ for component i of the

sample, to (iii) values of the drift correction function $\varepsilon_{drift}(t)$ at the times at which the sample was measured, and (iv) the pressure-corrected values A_i'(QA) and A_i'(sample) for component i of the QA and sample. (This transformation step involves the estimation of the parameters in a least-squares fit to the data for the QA followed by the evaluation of that fit at specific times.)

2. A transformation from (iii) and (iv) above to (v) the pressure-corrected values A_i'(QA) for component i of the QA, and (vi) the drift- and pressure-corrected values A_i''(sample) of component i of the sample.

3. A transformation from (v) and (vi) above to (vii) the average $\bar{A}_i'$(QA) of the pressure-corrected values for component i of the QA, and (viii) the average $\bar{A}_i''$(sample) of the drift- and pressure-corrected values for component i of the sample.

In terms of uncertainty propagation, each of the above steps can be described by a sensitivity matrix. The sensitivity matrix either represents the transformation of values exactly (in the case that the transformation is linear) or approximately (in the case that it is non-linear and the matrix is obtained by linearisation of the transformation). When linearisation is used, it may be necessary to assume nominal values for the quantities involved, *e.g.* the values of the drift correction function are nominally unity.

If it is assumed that the covariance matrix associated with the values in (i) and (ii) is proportional to the identity matrix, which is based on the assumptions that the values are uncorrelated and have the same associated variance, then the covariance matrix associated with the values in (vii) and (viii) can be determined up to a scale factor using a generalised (multivariate) version of the law of propagation of uncertainty. [12]

The values in (vii) and (viii) are then transformed to (ix) the (required) value of the ratio of the response factors for component i, RRF_i, of the sample and QA (equations 5, 6 and 7). The uncertainty propagation for this step can be undertaken with or without taking account of the covariance associated with the values $\bar{A}_i'$(QA) and $\bar{A}_i''$(sample). It is found that the standard uncertainty obtained taking account of the covariance is about 12 % greater than that obtained when that covariance is ignored.

Finally, a chi-squared test was used to check the internal consistency of the data sets. However, none of the data sets (with uncertainties at the $k = 2$ level) passed the chi-squared test, indicating that uncertainties for all *RRF* values were underestimated. Uncertainties in the y data were increased systematically for each data set by a factor such that each data set passed the chi-squared test with a 95 % confidence. These uncertainties were used then in the analysis of the variation of *RRF* with component amount fraction (see Section 4.1) and with molar weight (Section 4.2). As discussed in Section 4.2, robust methods were used in the analysis of the *RRF* as a function of the other physical properties instead, hence uncertainties in these cases were ignored.

3.6 UNCERTAINTIES IN AMOUNT FRACTIONS AND PHYSICAL PROPERTIES

Uncertainties in the gravimetric amount fractions of the components of each mixture were estimated in accordance with ISO 6142.[6] Relative standard uncertainties in the physical properties calculated using GasVLe were as recommended in ISO 12213-2:[13] 0.05 % for both density and molar volume, 2.5 % for viscosity. The uncertainty in the molar weight was the result of the combination of the uncertainties in the gravimetric amount fractions and of those in the molar mass of the components of each sample mixture, with the gravimetric component typically ~100 times greater than the molar mass component. The standard uncertainties in the molar weights were therefore dominated by the gravimetric uncertainty of each sample mixture, and were approximated to 0.05 %. The uncertainties described here are reported in Table 3, but were not ultimately used in the analysis of the data for reasons elucidated in Section 4.2.

4 RESULTS AND DISCUSSION

4.1 *RRF* AGAINST AMOUNT FRACTION

Plots of the *RRF* for methane, ethane, propane and the sum of *i*- and *n*-butane against the component amount fraction are shown in Figures 4a-d.

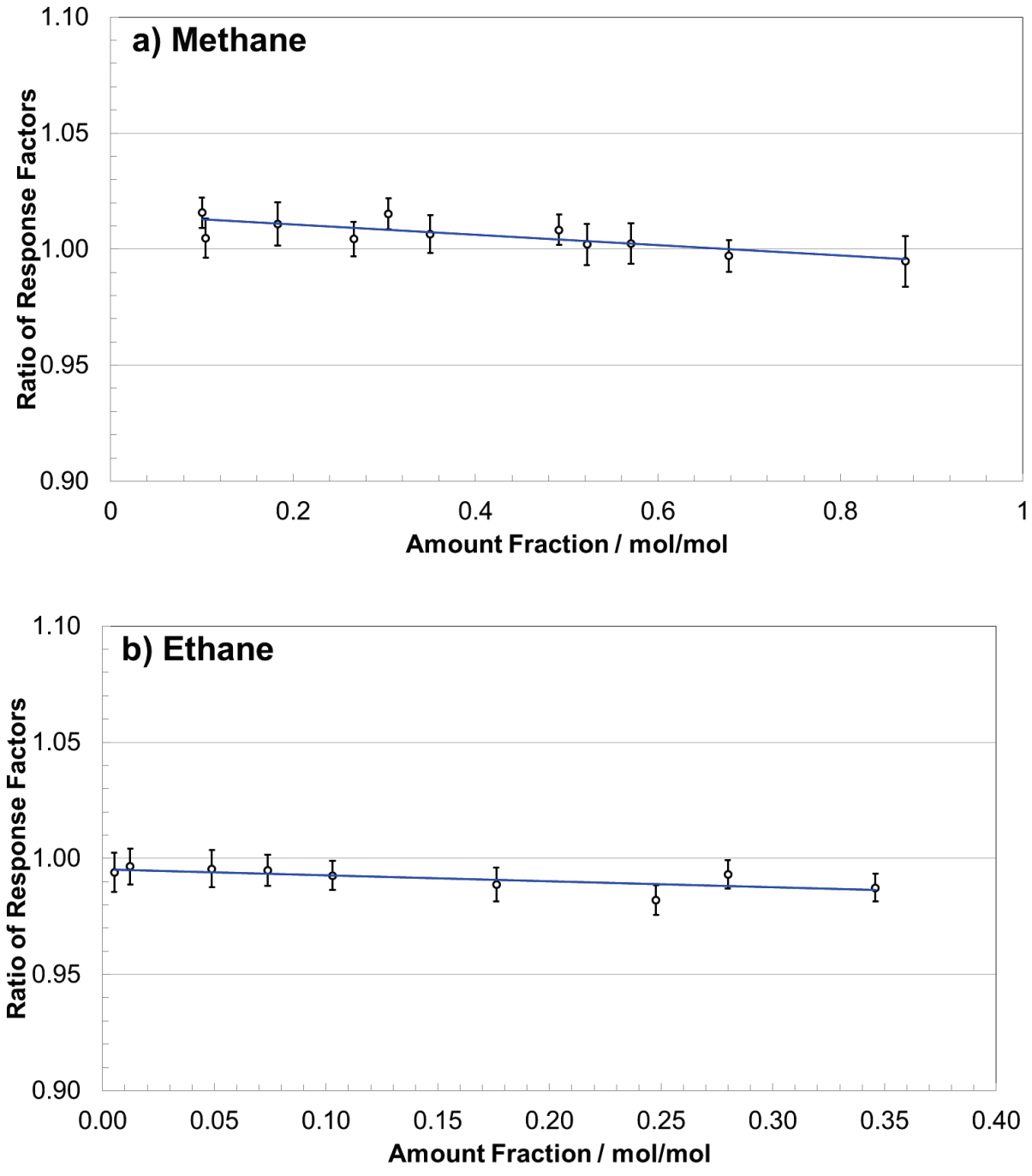

Figure 4 Plot of the *RRF* against amount fraction for a) methane and b) ethane. Uncertainties are at the $k = 2$ level; uncertainties in the values of amount fraction are too small to show graphically. OLS fits to the data are shown as solid blue lines.

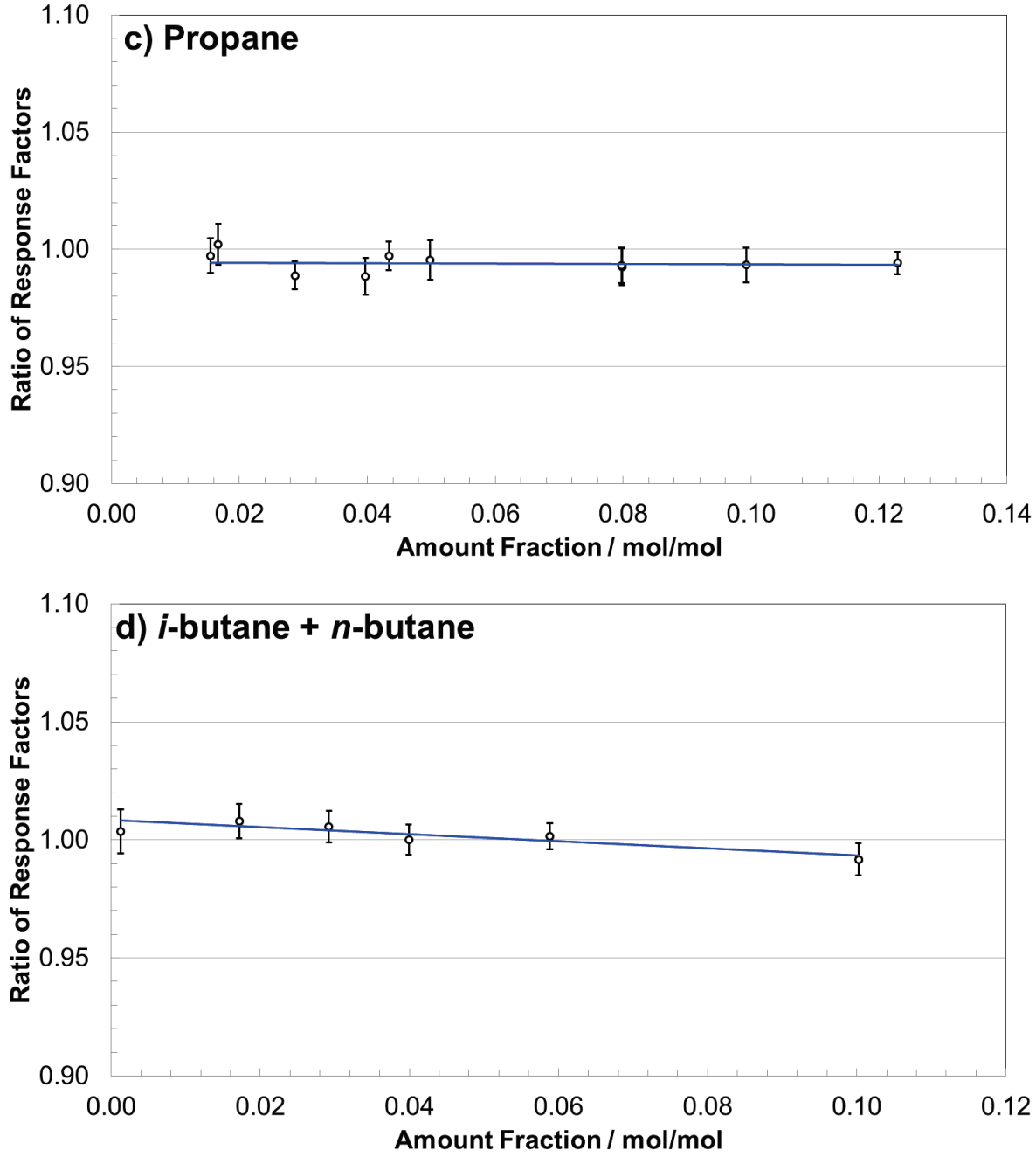

Figure 4 (*continued*) Plot of the *RRF* against amount fraction for c) propane and d) the sum of *i*-butane and *n*-butane. Uncertainties are at the $k = 2$; uncertainties in the values of amount fraction are too small to show graphically. OLS fits to the data are shown as solid blue lines.

All plots show that the *RRF* decreases with increasing amount fraction. To establish if such downward trends were statistically significant in the light of the uncertainties associated with the data points, a significance test was carried out as follows. Weighted linear fits to the plots of *RRF* against amount fraction were obtained for each component using NPL's XLGENLINE software.[14] The values of the gradient obtained from the fitting routine and its associated uncertainty were then analysed: if the uncertainty interval for the gradient of each plot at the $k = 2$ level encompassed zero, then a linear correlation between amount fraction and *RRF* could not be established and the trend in the data set could be said to be insignificant. Generalised least-squares (GLS) fits, using *x*- and *y*-weighted data, and ordinary least-squares (OLS) fits, using *y*-weighted data only, were both attempted on all plots of

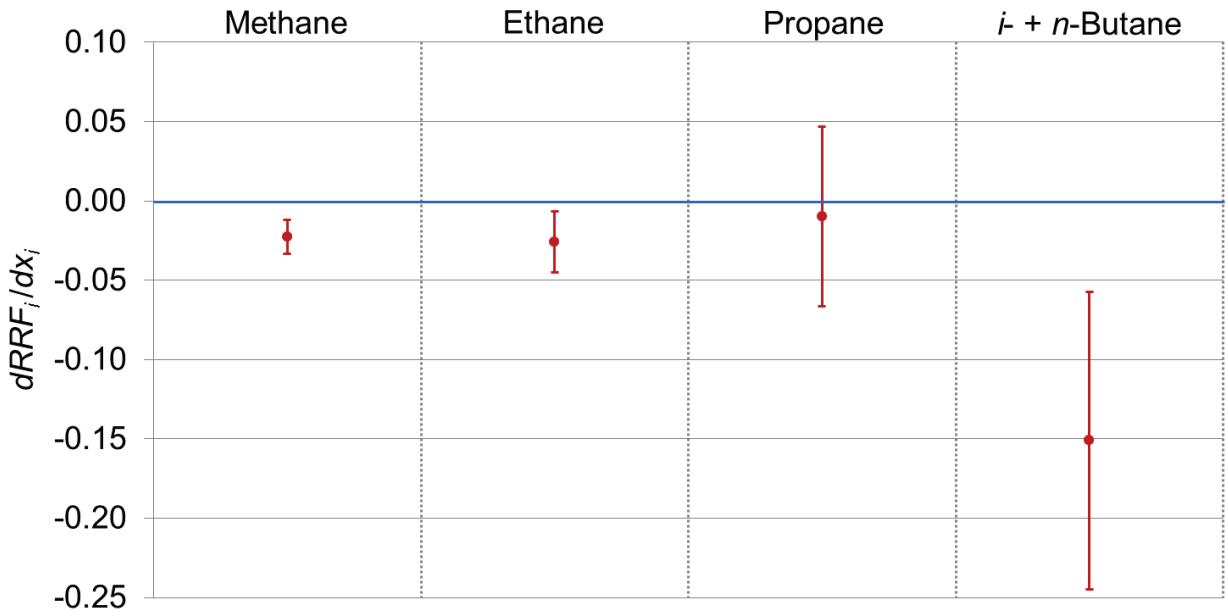

Figure 5 Significance analysis of plots of *RRF* against amount fraction for methane, ethane, propane and the sum of *i*- and *n*-butane. An overlap of the error bars (*k* = 2) with zero indicates no correlation between *RRF* and amount fraction.

RRF against amount fraction: as the uncertainties in the *RRF* were significantly greater than those in the amount fraction, the results from the GLS fits were identical to those from the OLS fits. The results of this analysis are shown in Figure 5: all components exhibit negative gradients ($dRRF_i/dx_i$) and only the uncertainty interval for the gradient from the propane data overlaps with zero. The uncertainty in the gradients obtained from fitting to the data for propane and the sum of the butanes are considerably larger than those obtained for methane and ethane, mainly because the interval of amount fractions over which the *RRF* for propane and the butanes were measured extended towards the limit of detection of the instrument. The *RRF* for methane was measured over the widest interval of amount fractions (0.10 to 0.87 mol/mol), over which it exhibited a change of –2 %. Similarly, the *RRF* for ethane exhibited a −0.7 % change over the amount fraction range 0.005 to 0.35 mol/mol. The *RRF* for propane and that for the sum of *i*- and *n*-butane were measured over a smaller interval of amount fractions (no higher than 0.12 mol/mol), over which they exhibited a change of respectively –0.3 % and –1.2 %. These results are not inconsistent with the trend exhibited by the response factors of propane and of the sum of *i*- and *n*-butane measured *via* FID on a different gas chromatography set-up (Agilent 7890A) at NPL: in that case, a change in response factor for synthetic natural gas mixtures of −0.6 % was observed for propane over the range 0.001-0.045 mol/mol and of −0.7 % for the sum of butanes over the range 0.0006-0.03 mol/mol.

In conclusion, a dependence of *RRF* on component amount fraction was observed for methane, ethane and the sum of the butanes, and this trend is typical of the non-linearity of an FID. However, the variation in *RRF* over the amount fraction interval typical of the components of the sample mixtures used in this study is minimal, as discussed above.

Other than the four components discussed above, hydrogen and nitrogen were also present in most sample mixtures over an appreciably broad range of amount fractions (up to 40-50 %): plots of *RRF* for methane, ethane, propane and the sum of *i*- and *n*-butane against hydrogen and nitrogen amount fractions were produced to investigate whether these two components had an effect on the FID response to those hydrocarbons; these plots are shown in Figures 6 and 7 respectively.

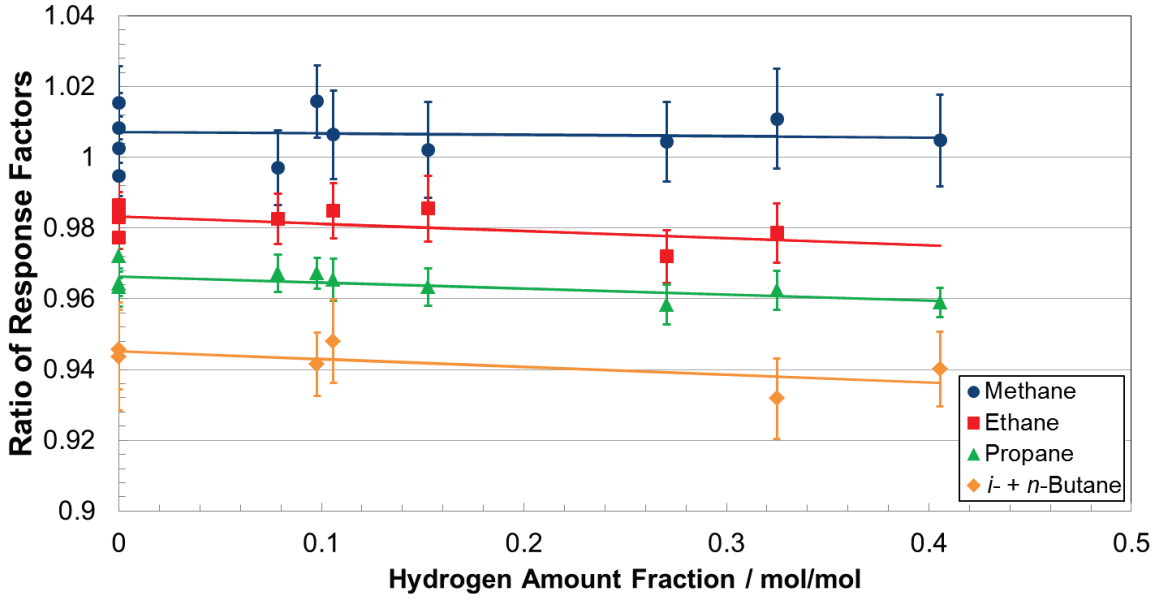

Figure 6 Plot of *RRF* against hydrogen amount fraction for methane, ethane, propane and the sum of *i*- and *n*-butane. Uncertainties are at the $k = 2$ level. OLS fits to each data series are shown as solid lines. The data for ethane, propane and the sum of *i*- and *n*-butane were offset by −0.01, −0.03 and −0.06 for clarity.

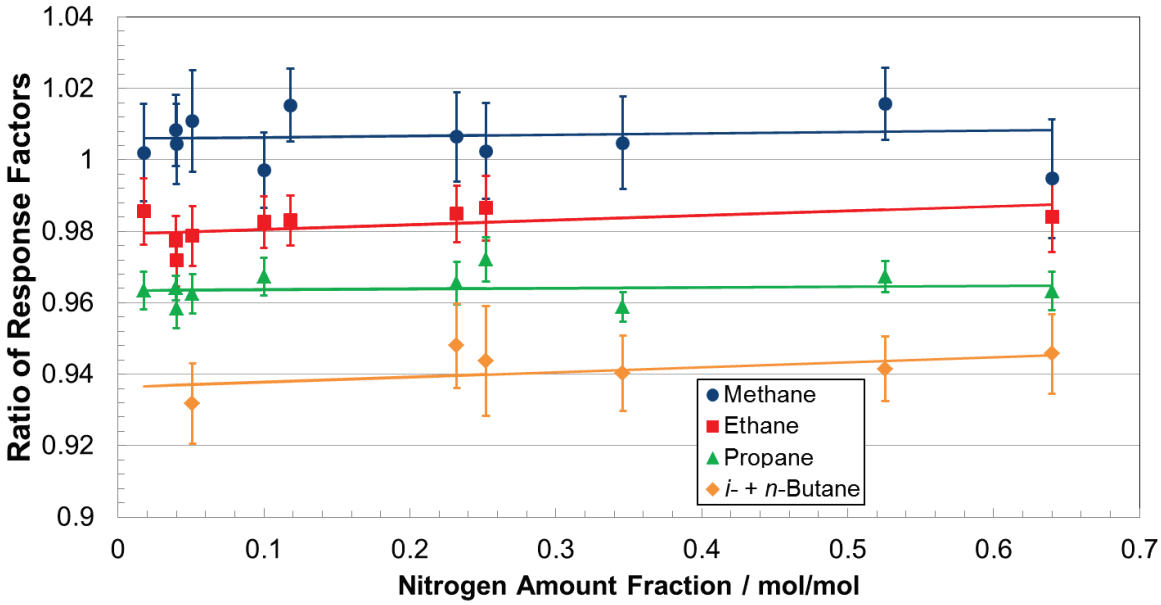

Figure 7 Plot of *RRF* against nitrogen amount fraction for methane, ethane, propane and the sum of *i*- and *n*-butane. Uncertainties are at the $k = 2$ level. OLS fits to each data series are shown as solid lines. The data for ethane, propane and the sum of *i*- and *n*-butane were offset by −0.01, −0.03 and −0.06 for clarity.

A significance analysis, analogous to the one carried out in Figure 4, was performed for the dependence of the *RRF* on hydrogen or nitrogen amount fraction. The results are shown in Figures 8 and 9 respectively. Of all the gradients, only that for the variation of the *RRF* of propane as a function of hydrogen amount fraction did not overlap with zero, indicating a possible correlation between these two variables. For the other seven relationships, no correlation between variables was found to exist.

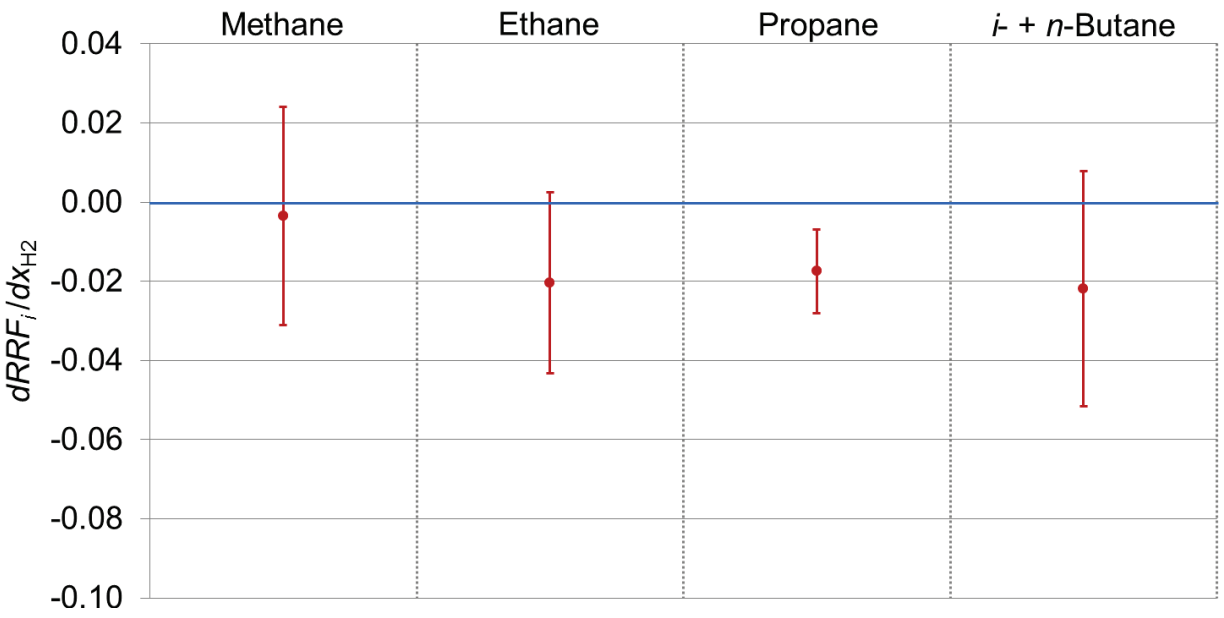

Figure 8 Significance analysis of plots of *RRF* against hydrogen amount fraction for methane, ethane, propane and the sum of *i*- and *n*-butane. An overlap of the error bars ($k = 2$) with zero indicates no correlation between *RRF* and amount fraction.

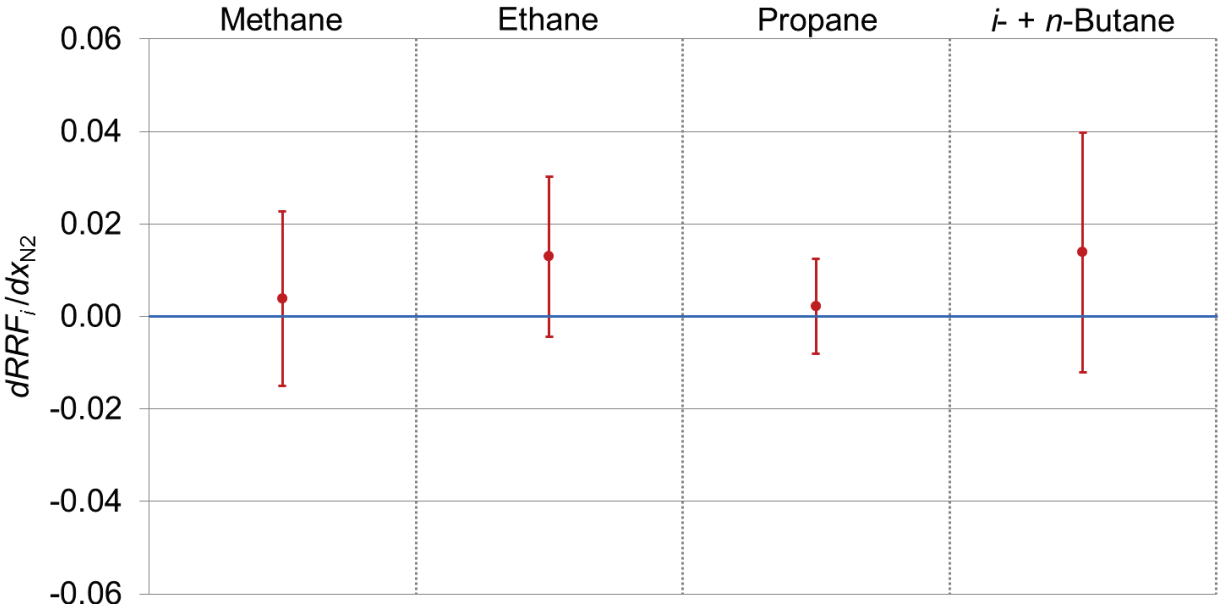

Figure 9 Significance analysis of plots of *RRF* against nitrogen amount fraction for methane, ethane, propane and the sum of *i*- and *n*-butane. An overlap of the error bars ($k = 2$) with zero indicates no correlation between *RRF* and amount fraction.

4.2 *RRF* AGAINST PHYSICAL PROPERTIES

The analysis of the effects of the physical properties of the sample mixtures on the *RRF* was somewhat less straightforward to address, as the four components considered for this study gave rise to four *RRF* values per sample mixture. Two analytical approaches could be envisaged: to either plot each component separately against each physical property (giving rise to 16 plots), or to average the *RRF* of different components within the same sample mixture (giving rise to only four plots). As it seemed

unlikely for a physical property to affect the *RRF* of one component in a different fashion from that of another (especially as the *RRF* values of all components exhibited very similar trends when plotted individually against each physical property), the first approach was not pursued. Plots of the averaged *RRF* against molar weight, molar volume, density and viscosity are illustrated in Figures 10, 11, 12 and 13 respectively; the individual *RRF* values (pre-averaging) are also shown for information.

Generalised least-squares (GLS) linear fits, weighted in both *x* and *y*, were attempted for each plot of *RRF* against a physical property using XLGENLINE. The software however was only able to successfully carry out a GLS fit for the plot of *RRF* against molar weight; for the three remaining plots, the software encountered a problem during the fitting routine and failed to converge to a solution. The failure was ascribed to the scatter of the data. Therefore the NPL software developed to support ISO/TS 28037:2010(E) [15] was used to fit to the data for the molar volume, density and viscosity: the programme did return optimised linear parameters from the fit, but it also flagged a failure of the chi-squared test, indicating that the validity of the assumption of a straight-line relationship between these quantities should be questioned. In the light of the failure of both pieces of software to fit to these three plots, along with the narrow width of the dynamic range of the corresponding three physical properties and the limited confidence in the estimate of the uncertainties in the *RRF* values (see Section 3.5), robust fitting routines were preferred over weighted least-squares fits for the plots of *RRF* against molar volume, density and viscosity. The robust analysis used was Theil's Incomplete Method: this is described extensively in the literature [16] and only a brief account is given here. Theil's Incomplete Method is a median-based technique which relies on calculating the gradients between pairs of points in the dataset: the median of the estimated gradients is then taken as the true gradient. The uncertainty in the median of the gradients is calculated as the standard deviation of the gradients obtained from pairs of data points.

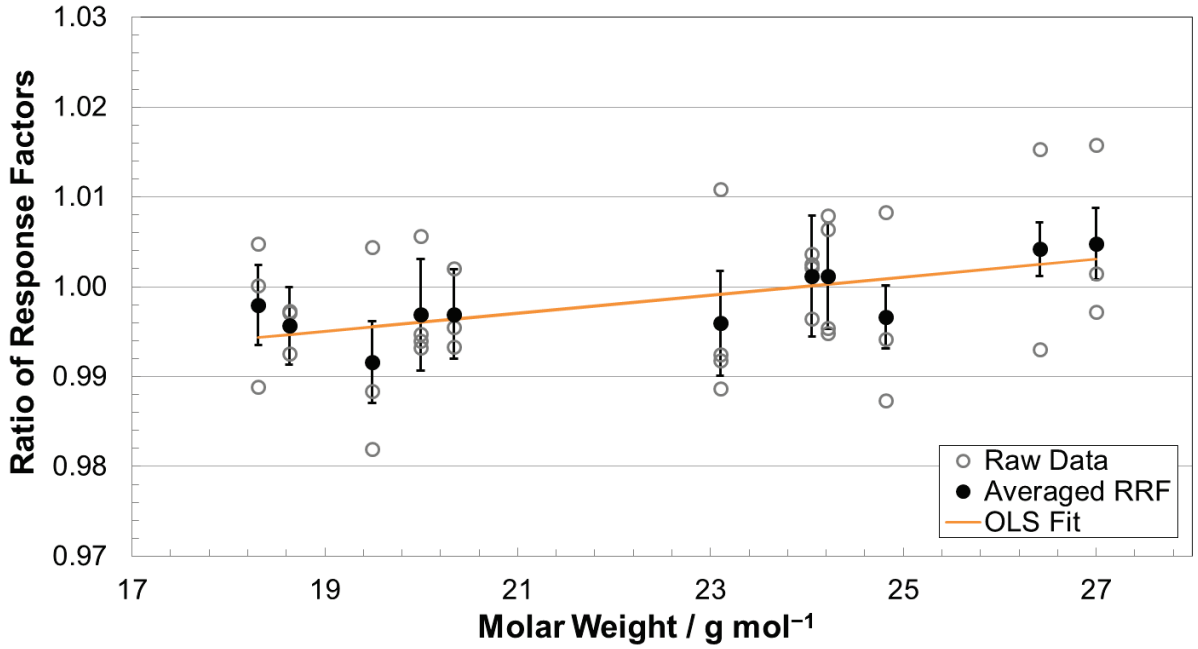

Figure 10 Effect of molar weight of the sample mixture on the normalised *RRF*. Individual *RRF* values from each sample are shown as open grey circles; the averaged *RRF* values for each mixture are shown as filled black circles. Error bars are at the *k* = 2 level. The solid orange line represents a GLS linear fit to the averaged *RRF* data.

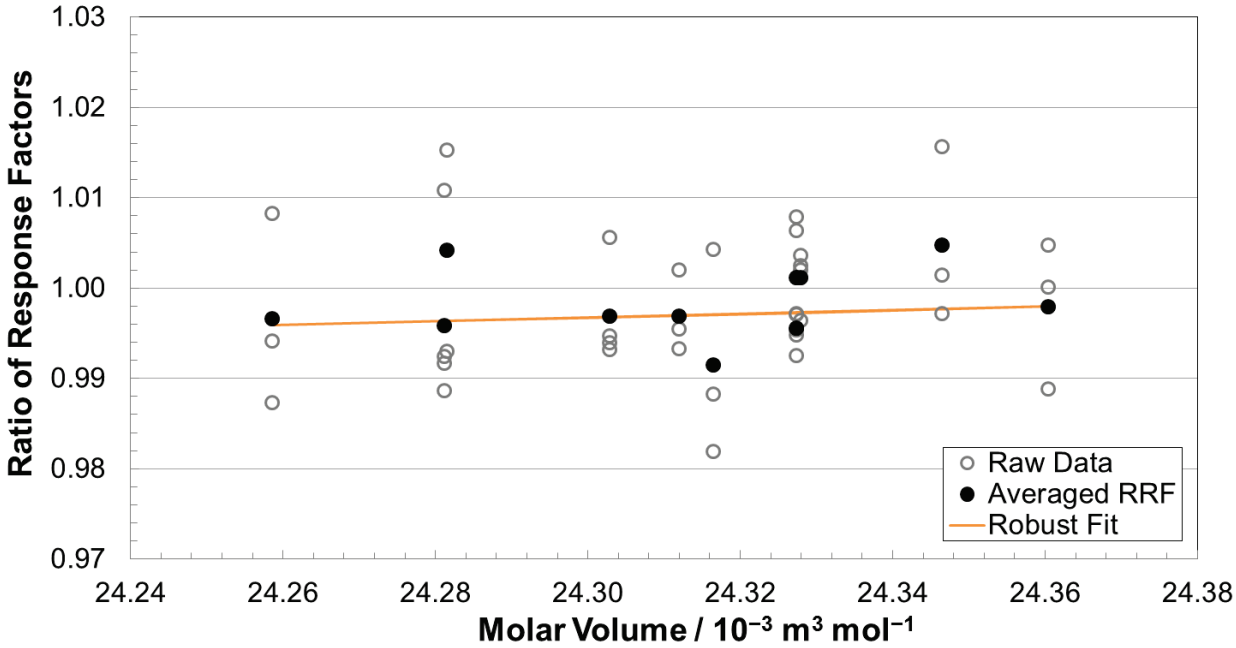

Figure 11 Effect of molar volume of the sample mixture on the normalised *RRF*. Individual *RRF* values from each sample are shown as open grey circles; the averaged *RRF* values for each mixture are shown as filled black circles. The solid orange line represents a robust linear fit to the averaged *RRF* data, obtained following Thiel's Incomplete Method.

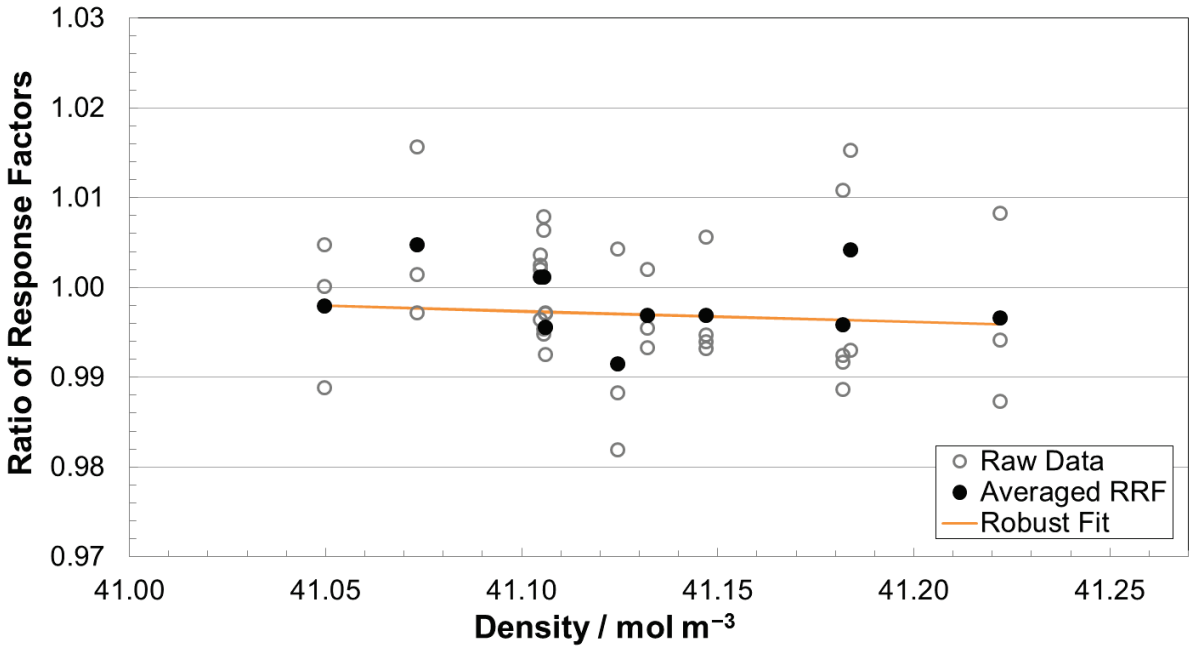

Figure 12 Effect of density of the sample mixture on the normalised *RRF*. Individual *RRF* values from each sample are shown as open grey circles; the averaged *RRF* values for each mixture are shown as filled black circles. The solid orange line represents a robust linear fit to the averaged *RRF* data, obtained following Thiel's Incomplete Method.

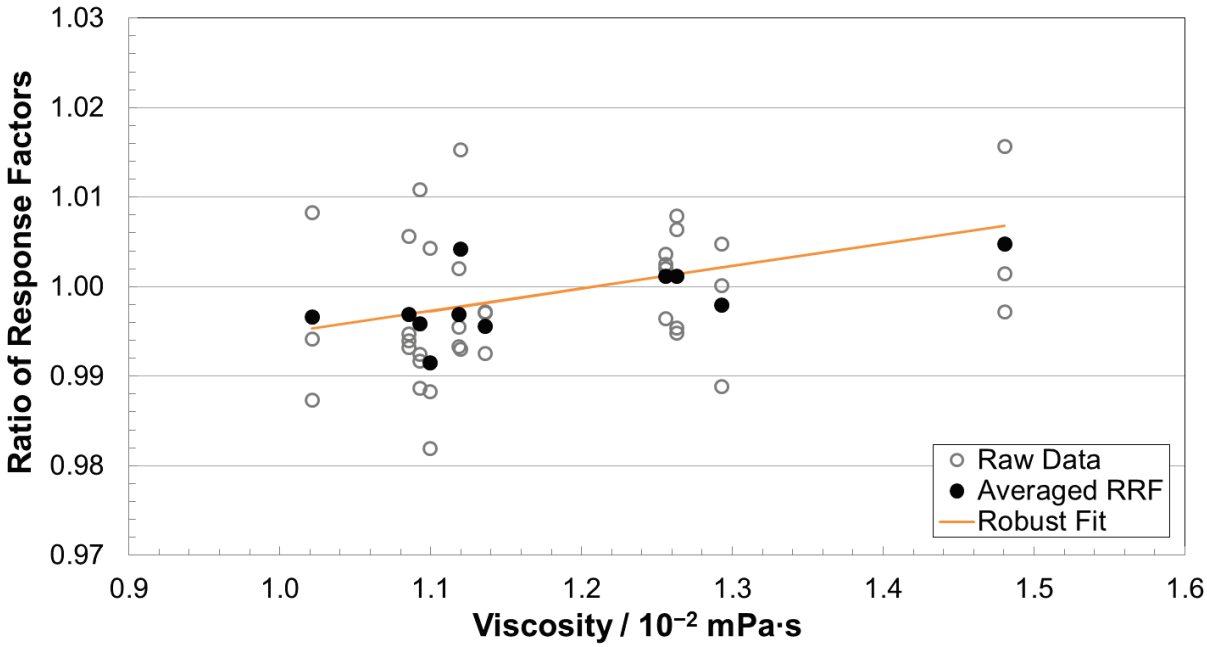

Figure 13 Effect of viscosity of the sample mixture on the normalised *RRF*. Individual *RRF* values from each sample are shown as open grey circles; the averaged *RRF* values for each mixture are shown as filled black circles. The solid orange line represents a robust linear fit to the averaged *RRF* data, obtained following Thiel's Incomplete Method.

A significance analysis analogous to the one performed for plots of *RRF* against component amount fraction was performed for the plots of *RRF* against physical properties of the sample mixtures: this procedure used the values of the gradient and its uncertainty from the XLGENLINE GLS fit for the molar weight data and those from the robust regression for the remaining three physical properties. As shown in Figure 14, the gradients of the fits to plots of *RRF* against molar volume, density and viscosity overlap with zero within the given uncertainty interval (k = 2), whereas that of the fit of *RRF* against molar weight does not. This significance analysis indicates the presence of a correlation between the *RRF* of methane, ethane, propane and of the sum of *i*- and *n*-butane and the overall molar weight of the gas mixture; more specifically, an increase in *RRF* with increasing molar weight was observed. However, it would be difficult to physically account for such an effect, and it could be envisaged how the correlation between the molar weight of a mixture and the component amount fraction (some of which have an effect on the observed *RRF*, as described in Section 4.1) could result in the dependence of *RRF* on molar weight shown in Figure 10. This possibility was explored by building a model that simulated the observed effect of molar weight on *RRF*: the *RRF* of each component was given a linear dependence on the amount fraction of the component itself (as shown in Figure 4a-4d) and on the amount fraction of hydrogen in the mixture (as shown in Figure 6), in such manner that an *RRF* surface was effectively defined. An unweighted multiple linear regression was performed so that a "best fit surface" was obtained for each component, as shown in Figure 15 for methane.

The best fit surfaces were used to obtain *RRF*s at values of the amount fraction of hydrogen and of the component of interest (methane, ethane, propane and butanes) specific to each sample mixture. The *RRF* obtained from components in the same mixture were then averaged and plotted against molar weight: as shown in Figure 16, the model and the experimental data are in very good agreement, indicating that the trend observed in *RRF* against molar weight is likely to arise from the correlation

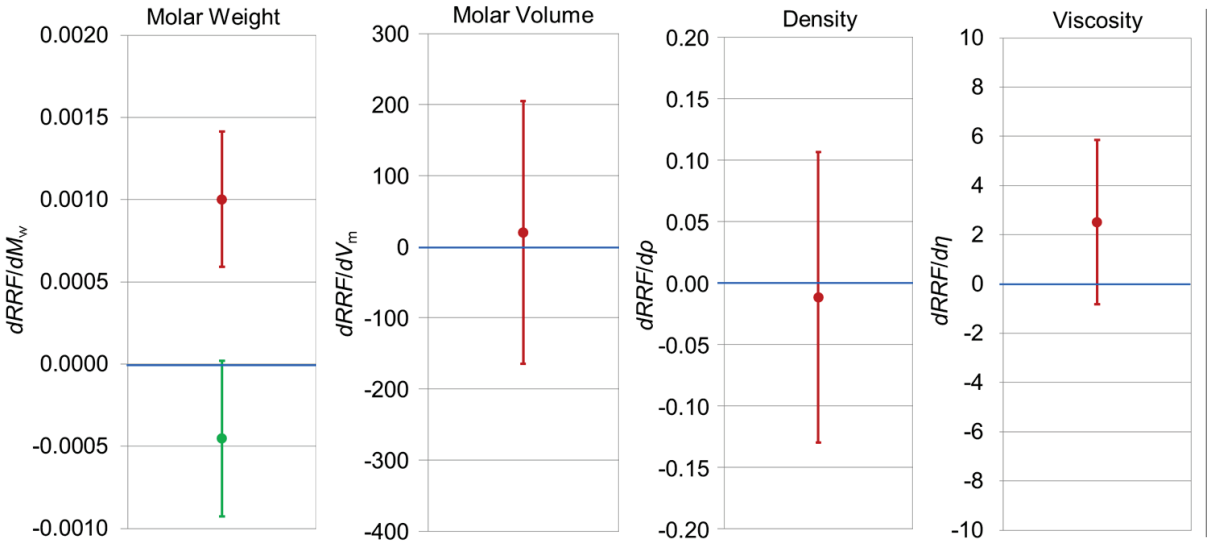

Figure 14 Significance analysis of plots of *RRF* against physical properties shown in red. An overlap of the error bars (k = 2) with zero indicates no correlation between *RRF* and the physical property. The data point in green in the panel for the molar weight was obtained from subtracting modelled data from the experimental values, as explained in detail in text.

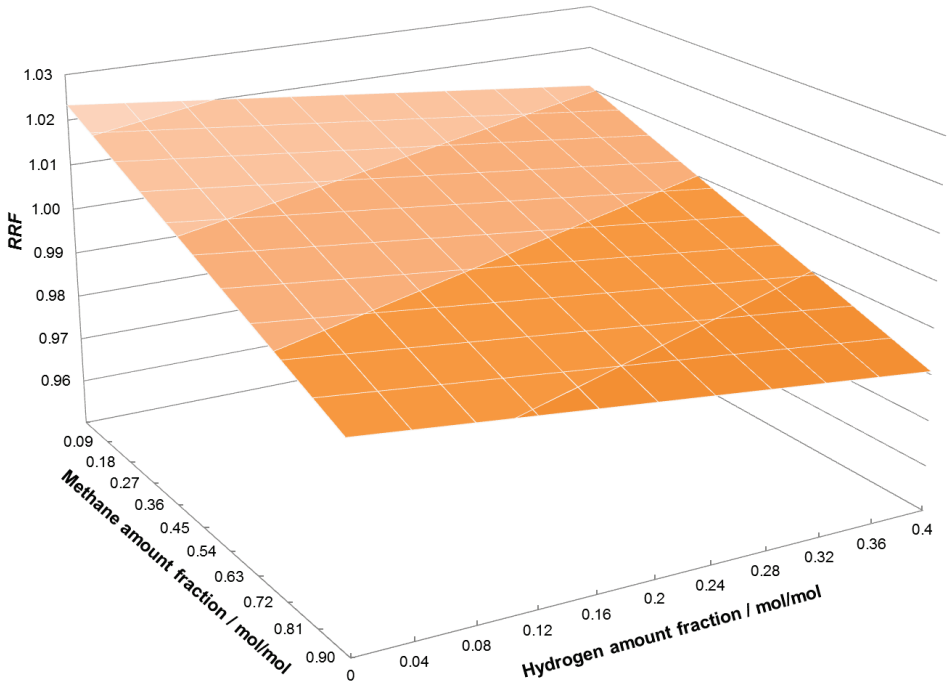

Figure 15 Best fit surface to the observed *RRF* data for methane as a function of methane and hydrogen amount fractions.

between molar weight and *RRF* values that are dependent on the amount fraction of some components. Subtraction of the results from the model from those obtained from experiments would in theory remove the effect of the dependence of *RRF* on component amount fractions: the residual would then show if a trend in *RRF* still persists, that could only be ascribed to the molar weight. When a GLS fit is attempted on the residual *RRF*, using the same uncertainty in the y-axis as the experimental *RRF* values, as shown in Figure 17, the resulting significance analysis plot showed that the gradient overlapped with zero, indicating that molar weight had a negligible effect on the *RRF* (Figure 14). It is

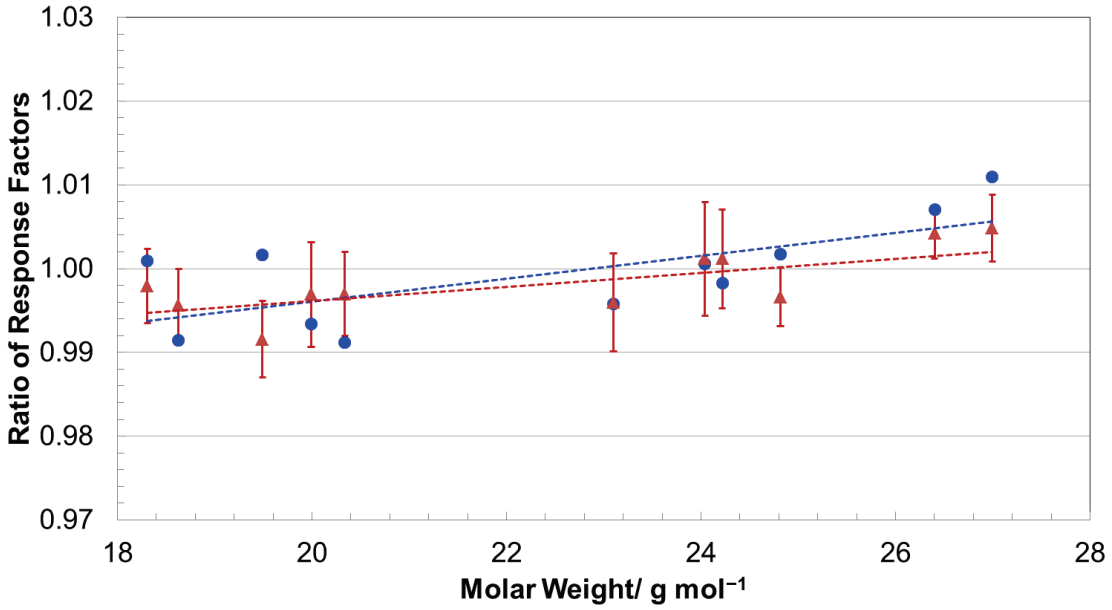

Figure 16 Plot of averaged *RRF* against molar weight; experimental data are shown as red triangles, whilst *RRF* values calculated from a model (see text) are shown as blue circles. Linear fits to both data sets (dashed lines) are also shown.

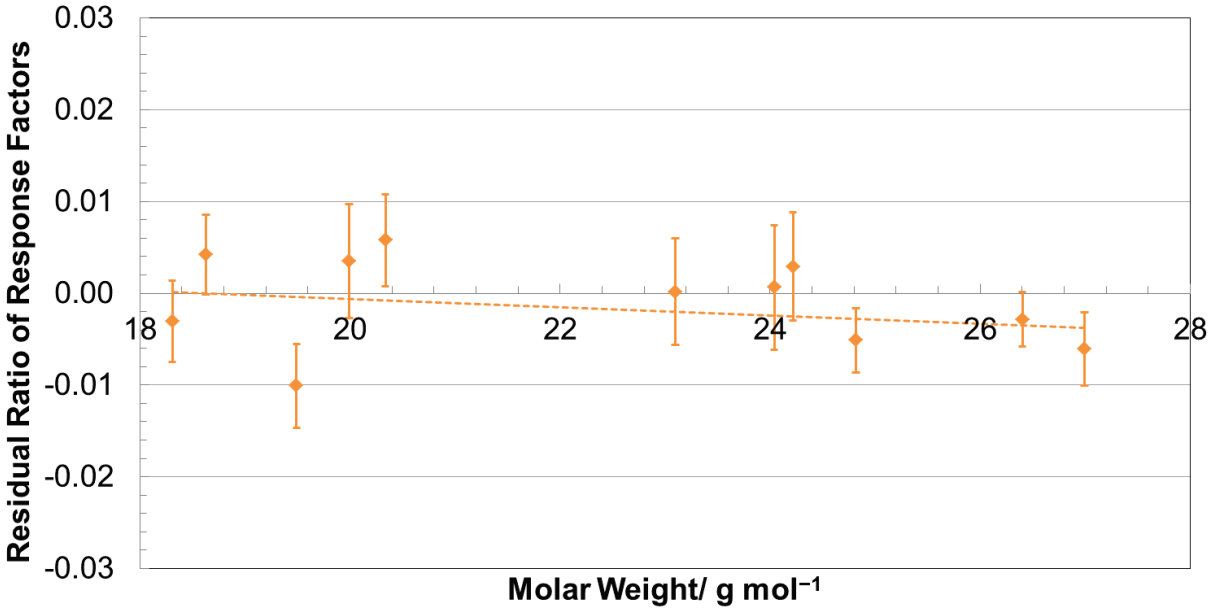

Figure 17 Plot of the residual *RRF* against molar weight; GLS fit to the data (dashed line) is also shown. Note that the error bars are of the same magnitude as those in Figure 16 no uncertainty has been assigned to the modelled data.

important to note that the error bars in the revised significance analysis for the plot of *RRF* against molar weight (green point in Figure 14) are effectively underestimated, as the error bars in the data points for the plot of residual *RRF* against molar weight in Figure 17 (and hence, the uncertainty of its gradient) assume that the modelled data have no uncertainty.

5 CONCLUSIONS

This work analysed the response of a gas chromatography set-up with FID (Refinery Gas Analyser) to methane, ethane, propane, *i*-butane and *n*-butane in a series of multi-component gas mixtures. The analysis of results showed significant impact of changes in atmospheric pressure and detector drift on the instrument response; a procedure to account for these effects was devised and it is recommended that pressure and drift corrections routines are adopted in future work performed on the Refinery Gas Analyser. It is most likely that the variations in response factors observed in preliminary experiments were caused by the absence of these corrections.

This work observed a minor dependence of the instrument response on the amount fraction of the hydrocarbons taken into account. As discussed above, this is not unusual and has been observed in the results obtained from other FIDs. However this study also observed a dependence of the response of one of the components studied (propane) to the hydrogen amount fraction of the mixture. As the physical process leading to the hydrogen amount fraction affecting the instrument response to only one component is difficult to account for, it cannot be excluded that the observed effect could be a manifestation of underestimated uncertainties in the data.

No significant effect of molar volume, density and viscosity on the instrument response was observed. A trend of increasing instrument response with increasing molar weight was however observed, but it was shown how this dependence most likely arose from the correlation with the dependence of the instrument response on the amount fraction of some components within the mixtures.

6 REFERENCES

[1] Directive 2003/87/EC of the European Parliament and of the Council of 13 October 2003 establishing a scheme for greenhouse gas emission allowance trading within the Community and amending Council Directive 96/61/EC, *Official Journal of the European Union*, **2003**, *46*, L275/32-L275/46

[2] BS EN 15984:2011, *Petroleum industry and products – Determination of composition of refinery heating gas and calculation of carbon content and calorific value – Gas chromatography method*

[3] G. Nieuwenkamp, R.M. Wessel, A.M.H. van der Veen, P.R. Ziel, Q. Han, D. Tuma, J.-C. Woo, J. Tóthné Fuko, N. Szilágyi, T. Büki, L.A. Konopelko, Y.A. Kustikov, T.A. Popova, V.V. Pankratov, M.N. Pir, E.V. Nazarov, L.V. Ehvalov, A.U. Timofeev, T.A. Kuzmina, A.V. Meshkov, M. Valkova, V. Pätoprsty, M. Downey, G. Vargha, A. Brown, M. Milton, *Metrologia*, **2012**, *49*, 08003

[4] Analytical Controls, HiSpeed RGA User Manual, Version 2007/1.0

[5] A.S. Brown, *GravCalc2 (version 2.3.0) User Guide*, **2009**, NPL Report AS 42, Teddington, UK

[6] ISO 6142:2006, *Gas Analysis – Preparation of Calibration Gas Mixtures – Gravimetric Methods*

[7] O. Redlich , J.N.S. Kwong, *Chem. Rev.*, **1949**, *44*, 233–244

[8] G. Soave, *Chem. Eng. Sci.*, **1972**, *27*, 1197-1203

[9] M.L. Salit, G.C. Turk, *Anal. Chem.* **1998**, *70*, 3184-3190

[10] NPL online barograph, http://resource.npl.co.uk/pressure/pressure.html

[11] BIPM, IEC, IFCC, ILAC, ISO, IUPAC, IUPAP and OIML, *Guide to the expression of uncertainty in measurement (GUM:1995 with minor corrections)*, **2008**, Bureau International des Poids et Mesures, JCGM 100

[12] BIPM, IEC, IFCC, ILAC, ISO, IUPAC, IUPAP and OIML, *Evaluation of measurement data–Supplement 2 to the 'Guide to the expression of uncertainty in measurement'–Extension to any number of output quantities*, **2011**, Bureau International des Poids et Mesures, JCGM 102

[13] BS EN ISO 12213-2:2009, *Natural gas – Calculation of compression factor part 2: Calculation using molar composition analysis*

[14] I. Smith, *Software for determining polynomial calibration functions by generalised least squares: user manual*, **2010**, NPL Report MS 11

[15] ISO Technical Specification (TS) 28037:2010(E) *Determination and use of straight-line calibration functions*

[16] Analytical Methods Committee, AMCTB No. 50, *Anal. Methods*, **2012**, *4*, 893–894